The visual cortex produces a signal in the gamma band in response to broadband visual flicker

Alexander Zhigalov[1], Katharina Duecker[1] and Ole Jensen[1]

[1]Centre for Human Brain Health, School of Psychology, University of Birmingham, B15 2TT Birmingham, United Kingdom

Abstract

The aim of this study is to uncover the network dynamics of the human visual cortex by driving it with a broadband random visual flicker. We here applied a broadband flicker (1–720 Hz) while measuring the MEG and then estimated the temporal response function (TRF) between the visual input and the MEG response. This TRF revealed an early response in the 40–60 Hz gamma range as well as in the 8–12 Hz alpha band. While the gamma band response is novel, the latter has been termed the alpha band perceptual echo. The gamma echo preceded the alpha perceptual echo. The dominant frequency of the gamma echo was subject-specific thereby reflecting the individual dynamical properties of the early visual cortex. To understand the neuronal mechanisms generating the gamma echo, we implemented a pyramidal-interneuron gamma (PING) model that produces gamma oscillations in the presence of constant input currents. Applying a broadband input current mimicking the visual stimulation allowed us to estimate TRF between the input current and the population response (akin to the local field potentials). The TRF revealed a gamma echo that was similar to the one we observed in the MEG data. Our results suggest that the visual gamma echo can be explained by the dynamics of the PING model even in the absence of sustained gamma oscillations.

Introduction

The properties of the neuronal dynamics governing the visual system are highly debated. Some emphasize the neuronal firing rate [1–3] and evoked activity [4] in response to visual stimuli. Others emphasize the oscillatory neuronal dynamics. In particular, neuronal oscillations in the gamma band have been proposed to bind visual features by means of synchronized spiking [5,6] as well as supporting communication between different brain regions [7,8].

In this paper we are applying a new tool for investigating the dynamical properties of the visual cortex in humans. We are making use of a new type of LED/DLP projector (Propixx, VPixx Technologies Inc., Canada) that has a refresh-rate of up to 1440 Hz. The projector makes it possible to stimulate the visual system with broadband flickering stimuli while measuring the brain response using magnetoencephalography (MEG). This approach allows for estimating the temporal response function (TRF). The TRF is the kernel that best explains the brain response when convolved to the broadband input signal. In other words, the TRF can be considered a simple model capturing the filter properties of the visual cortex. In previous studies, such an approach has been used to investigate the dynamical properties of the visual system at lower frequencies. Using a broadband flicker (1–80 Hz), the TRF was approximated from the cross-correlation between the EEG and the input signal [9]. This approach revealed a robust response in the alpha range termed “the perceptual echo”. Yet, the authors did not report dynamical properties in the gamma range most likely due to the limited refresh rate of the monitor [9]. The aim of this study was to ask if the TRF also has a

band-limited response at higher frequencies, to uncover the faster dynamical properties of the visual system. As we will show, the TRF function has a clear response at higher frequencies which is limited to the gamma band.

The oscillatory dynamical properties of the cortical tissue have also been investigated by means of computational modelling. This has resulted in the notion that neuronal gamma oscillations are generated by the so-called pyramidal interneuron gamma (PING) mechanism [10–12]. According to this mechanism, GABAergic interneurons play an essential role in determining the frequency and synchronization properties for the generation of gamma oscillations. Basically, the decay of the GABAergic feedback is a key variable determining the period of each gamma cycle as the GABAergic hyperpolarization prevents neuronal firing of both pyramidal and interneurons of about 10-20 ms [13]. Furthermore, the GABAergic feedback also serves to synchronize the population activity [14,15] The pyramidal neurons also play an important role in the mechanism. In each cycle, the firing of the pyramidal cells serve to excite the interneurons thus initiating the next oscillatory cycle. This mechanism was first uncovered in hippocampal rat slices [16] and supported by computational modelling [10–12]. Later, the GABAergic based mechanism was also investigated using optogenetic studies in the somatosensory cortex [17,18] and the visual system [19] in mice. A human MEG study demonstrated that gamma oscillations are strongly modulated after the GABAergic feedback was manipulated by the GABAergic agonist lorazepam in a double-blind study. As predicted by the PING model, the visual gamma oscillations decreased in frequency while they increased in power as the GABAergic feedback increased with the administration of lorazepam [20]. Other studies have reported a link between gamma frequency and the GABA concentration as measured by magnetic resonance spectroscopy (MRS) in both visual and somatosensory regions [21–23] (but see [24]). Finally a PET study measuring GABA(A) receptor density found a link to gamma frequency [25].

In this study, we asked if the dynamical properties of the PING model can account for the gamma response in the TRF we observed in the MEG data. The basic idea was to simulate a network model for gamma oscillations with a broadband signal. This allowed us to estimate the TRF of the network model and relate it to the TRF from MEG study. If the network model can procure a TRF similar to the one observed in the MEG data, then we have provided novel insight on the neuronal dynamics governing the early visual system.

In short, to investigate the dynamical properties of the visual system, we recorded the MEG while stimulation the visual system using a broadband (1–720 Hz) visual flicker. This allowed us to estimate the TRF of the visual system. As we will demonstrate, this resulted in a clear band-limited response in the gamma band. We then constructed a physiologically realistic network model that could generate gamma-band oscillations by a PING-type mechanism. This model allowed us to account for empirically observed TRF in the gamma band.

Methods

Participants

Five participants (mean age: 33; age range: 28-38; 1 female) with no history of neurological disorders partook in the study. The study was approved by the local ethics committee (University of Birmingham, UK) and written informed consent was acquired before enrolment in the study. All participants conformed to standard inclusion criteria for MEG experiments. Participants had normal or corrected-to-normal vision.

Experimental paradigm

Two moving grating stimuli were presented bilaterally (Fig. 1A). The participants were instructed to focus on the fixation point and press the button when a cue indicating the direction of motion (i.e. coherent or incoherent) occurred at the fixation point. The grating stimuli moved at a constant speed of 0.5 degree/s, and the stimuli were on for 3 s. The luminance of the stimuli was modulated using a broadband (i.e. noise with uniform distribution) flickering signal (Fig. 1B). The broadband signals for the left and right stimuli were uncorrelated (the correlation was below 0.01). We used the PROPixx DLP LED projector (VPixx Technologies Inc., Canada) to present the visual stimuli at a high refresh rate of 1440 Hz with a resolution of 960 x 600 pixels (see, [26]). The experimental paradigm was implemented in MATLAB 2017a (Mathworks Inc., Natick, USA) using Psychophysics Toolbox 3.0.11 [27].

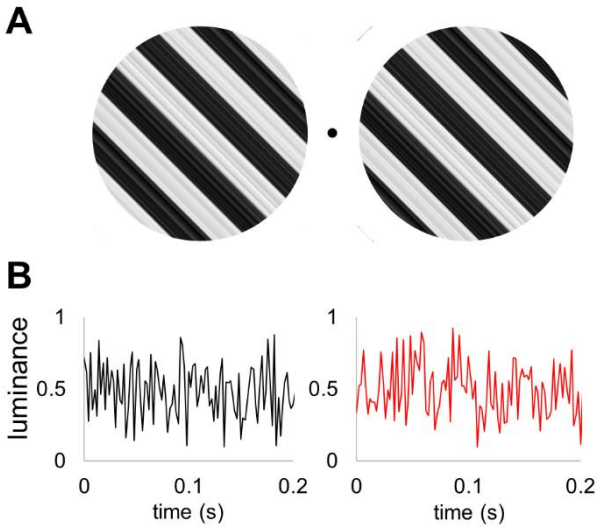

Fig. 1. Experimental paradigm. A) Two grating stimuli with either coherent or incoherent motion were presented bilaterally. Motion started 0.5 s after the onset of the flickering stimuli and lasted for 3 s. (B) Luminance of the left and right grating stimuli was modulated by two independent broadband signals.

Magnetoencephalography data processing

The MEG data were acquired using a 306-sensor TRIUX Elekta Neuromag system (Elekta, Finland). The magnetic signals were bandpass filtered from 0.1 and 330 Hz using embedded anti-aliasing filters and then sampled at 1000 Hz. The acquired time series were segmented into 4 s epochs; −1 to 3 s relative to the onset of the stimuli motion. Simultaneously with the MEG, we also acquired the eye-movements and blinks using an EyeLink eye-tracker (SR Research, Canada). Eye blinks were detected in the X-axis and Y-axis channels of the eye tracker by applying a threshold of 5 SD. The saccades were detected using a scatter diagram of X-axis and Y-axis time series of the eye-tracker for each trial. An event was classified as a saccade if the focus away from the fixation point by 2° and lasted longer than 500 ms. Trials contaminated by blinks and saccades were removed from further analysis. We also rejected trials containing large-amplitude events (above 5 SD) in MEG which are mainly associated with motion and muscle artefacts. As a result, the number of trials that remained after exclusion was 142 ± 10 (mean ± SD) per participant. For each participant, the number of trials per condition was equalized by randomly selecting the same number of trials.

Power spectral density

The power spectral density was estimated using Welch's method as implemented in the SciPy toolbox [28]. To this end, the 5 s epoch of data was divided in 1 s segments with 50% overlap and weighted by a Hanning window. The same approach was applied to estimate the power spectral density of the modelled data.

Temporal response functions

Temporal response functions (TRF) were estimated using ridge regression as implemented in mTRF toolbox [29]:

$$TRF = (S^T S + \lambda I)^{-1} S^T x$$

where *S* is the lagged time series of the stimulus, *x* denotes neuronal response, *I* is the identity matrix, and *λ* is the smoothing constant or "ridge parameter". In this study, the smoothing constant *λ* was set to 1.

The TRF were computed between the broadband flickering signal and the MEG gradiometer with the strongest visual flicker response. In order to assess contribution of 50 Hz line noise to the TRF, we also computed the TRF for MEG magnetometer with strongest response to the visual flicker before and after applying source space separation (SSS) method [30] for noise reduction. For the modelled data we calculated the TRF between the broadband input current and the mean membrane potential for the E-cells.

Time-frequency analysis

The time-frequency representations of power of the TRF were computed using Hanning tapper approach as implemented in Fieldtrip toolbox [31]. We used time-windows of different length spanning 5 cycles at the specific frequency. The analysed frequency range was 5–100 Hz with steps of 1 Hz and the time ranged from -0.1 to 0.2 (or 0.7 as in Figure 1) seconds with steps of 5 ms.

Model

We modelled the neuronal populations of cortical areas as a network of interconnected excitatory and inhibitory neurons (Fig. 2A). The network model was composed of 160 regular spiking excitatory pyramidal neurons (E-cells), and 40 fast-spiking inhibitory interneurons neurons (I-cells).

Neuronal model

We used the neuronal model proposed by Izhikevich [32] to simulate the membrane potentials of the excitatory and inhibitory neurons.

$$v' = 0.04v^2 + 5v + 140 - u + I + I_{syn} \quad (1)$$

$$u' = a(bv - u) \quad (2)$$

$$s'_{AMPA} = \alpha_{AMPA} F(v)(1 - s_{AMPA}) - \beta_{AMPA} s_{AMPA} \quad (3)$$

$$s'_{GABA} = \alpha_{GABA} F(v)(1 - s_{GABA}) - \beta_{GABA} s_{GABA} \quad (4)$$

where *v* represents the membrane potential of the simulated neuron, *I* determines the input current, *u* is a slow recovery variable. The model also includes a reset: when *v* exceeds 30 mV, an action potential is assumed, and the variables are reset: *v* = *c* and u = u + d. The

coefficients a = 0.02 and b = 0.2, c = -65 and d = 8 define the regular spiking E-cells, while a = 0.1 and b = 0.2 c = -65 and d = 2 define the fast spiking I-cells. The variable *s* represents the gating for synaptic input and includes both s_{AMPA} and s_{GABA} defined for each sending E-cell and I-cell, respectively.

To model the kinetics of the AMPA and GABA neurons, we followed the formalism from Wang and Buszaki [11].

The term I_{syn} reflects the synaptic current in the receiving neurons whereas *s* reflects the gating variable in the sending neuron,

$$I_{syn} = \sum_{i=1}^{N} C_{(:,i)} \cdot s_{AMPA} \cdot (v_{AMPA} - v) + \sum_{j=1}^{M} C_{(:,j)} \cdot s_{GABA} \cdot (v_{GABA} - v) \quad (5)$$

where N is the number of excitatory neurons, M is the number of inhibitory neurons, C is the connectivity matrix, v_{AMPA} and v_{GABA} are reversal potentials of AMPA (v_{AMPA} = 0 mV) and GABA receptors (v_{GABA} = -70 mV on E-cells and v_{GABA} = -75 mV on I-cells), respectively. The differential equation (3 and 4) includes parameters channel opening rate α_{AMPA} = 12 (ms^{-1}) and the channel closing rate β_{AMPA} = 0.5 (ms^{-1}) for AMPA receptors, and α_{GABA} = 12 (ms^{-1}) and β_{GABA} = 0.1 (ms^{-1}) for GABA receptors; *F* denotes a sigmoid function: $F(v) = 1/\left(1 + exp(-v/2)\right)$.

Connectivity between E-cells and I-cells was bidirectional, and the connection weights (or connection strength) between E-cells (c_{ee}), between I-cells (c_{ii}) as well as from E-cells to I-cells (c_{ei}), and from I-cells to E-cells (c_{ie}) were specified in the connectivity matrix C = [c_{ii}, c_{ie}; c_{ei}, c_{ee}] (see, Fig. 3A). The specific connectivity weights between excitatory and inhibitory neurons were adjusted to maximize the robustness of the oscillations, and the following values were used c_{ee} = 0.001, c_{ii} = 0.200, c_{ei} = 0.050, c_{ie} = 0.010. Additionally, each element in the connectivity matrix was multiplied with random values drawn from a uniform distribution to ensure heterogeneous connectivity (range [0, 1]) (see, Fig. 3A).

Population activity and local field potential produced by the model

The population activity of the model reflecting the local field potentials was computed by summing the membrane potentials of the E-cells. This somehow approximates the fields measured by MEG which are generated by the sum of dendritic currents in pyramidal cells [33].

To solve the differential equations (1-4) numerically, we used the Euler method with the time-step Δt = 1 ms.

Results

We used a moving grating paradigm in which the left and right visual stimuli were generated using orthogonal broadband random signals while we recorded the ongoing MEG (Fig. 1).

Broadband visual stimulation reveals alpha and gamma echoes in the visual system

The temporal response function (TRF) of a system can be estimated by deconvolving its input and output [29]. We used ridge regression (see, Methods) to compute the TRF for the MEG signals from sensors over visual cortex while stimulating with a broadband random visual input. Figure 2 shows the TRF for an occipital sensor for a representative participant. The TFR has a rich temporal structure (Fig. 2A, black line). Applying a bandpass filter in the gamma band (40–100 Hz) to the TRF revealed an early response (Fig. 2A, blue line) at

about 40 ms. A bandpass filter in the alpha band (8–13 Hz) revealed a later response comprising several cycles. A time-frequency analysis of power further demonstrated the presence of band-limited responses in the alpha and gamma band in the TRF (Fig. 2B). While the late response – the ”alpha perceptual echo” – was reported in the previous studies (e.g. [9], the early response – the ”gamma echo” – is so far unobserved property of the visual system.

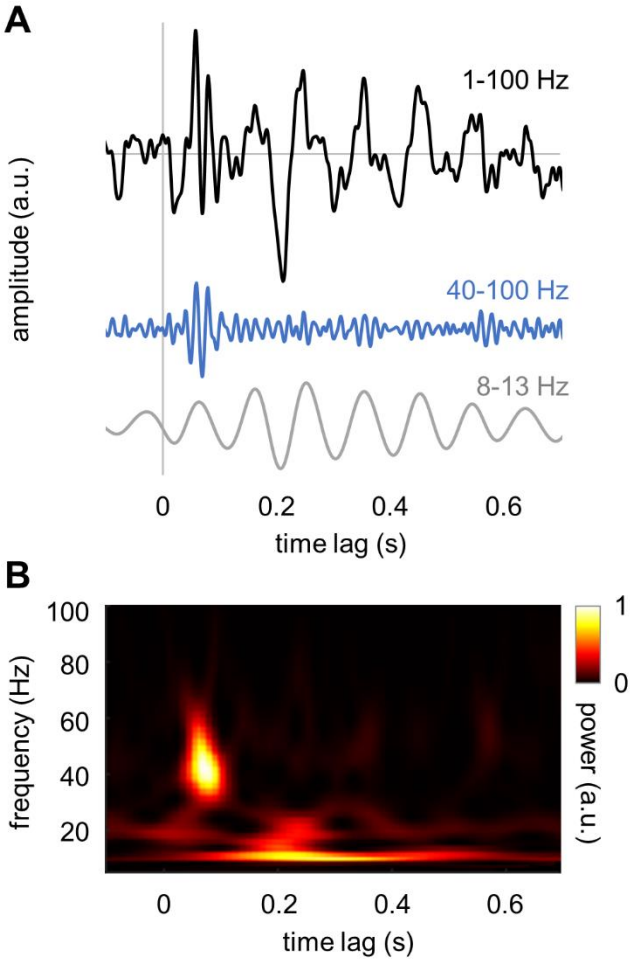

Fig. 2. TRF of the human visual cortex derived from a random broadband visual input train. (A) The TFR filtered in the broad band (1–100 Hz; black line), the gamma band (40–100 Hz; blue line) and the alpha band (8–13 Hz; gray line). (B) Time-frequency representation of power of the TRF.

TRF show individual resonance frequency of gamma echo

To further evaluate the characteristics of the gamma echo, we computed TRF for five individual participants using the MEG gradiometers with strongest response to the broadband input signal. The frequencies of the individual gamma echoes ranged from 46 to 56 Hz and were close to 48 Hz on average (Fig. 3). As we will discuss later these differences exclude that the response in the gamma band is a consequence of 50 Hz line noise. The response in the gamma band were strongest at 50 – 100 ms with a duration of 2 –3 cycles.

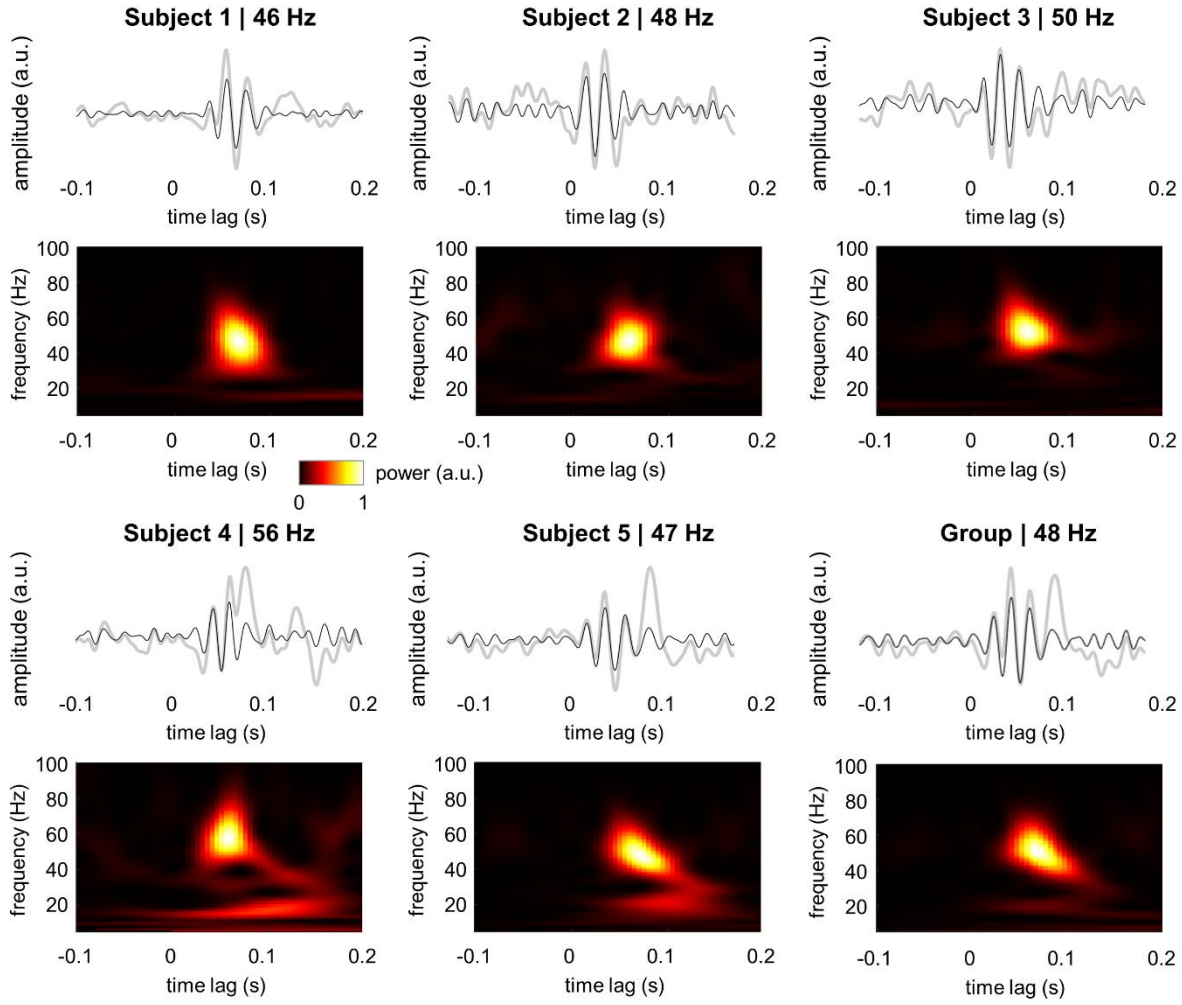

Fig. 3. TRF and the associated time-frequency representation of power for individual participants. Note the robust response in 40–60 Hz gamma range. Gray lines depict the TFR at 1–100 Hz while the black lines show the response filtered at 40–100 Hz.

The gamma echo is close to 50 Hz but not due to line noise

To ensure that the 50 Hz line noise does not contribute to the gamma echo, we assessed the power spectral density and TRF for magnetometers before and after applying the source space separation (SSS) method [30] as implemented in MNE Python toolbox [34]. SSS removes artifacts caused by external disturbances such as line noise, and hence, provides possibility to evaluate contribution of 50 Hz noise to the gamma echo. We performed the analysis on the magnetometers as they are particularly sensitive to 50 Hz line noise and hence, they provide a worst case setting. The results clearly showed that suppression of 50 Hz noise in data did not change the characteristics of gamma echo (Fig. S1) in any of the participants. This demonstrates that the gamma echo is not biased by line noise.

PING based model of gamma oscillations

We implemented a pyramidal-interneuron gamma (PING) [10,12,16] network model with biologically plausible synaptic currents [11] attempting to account for the TRF in the gamma band. The model consisted of interconnected excitatory (E) and inhibitory (I) cells (Fig. 4A).

The connectivity matrix in Fig. 4B describes the connection strengths between all the cells. In this model, we used a relatively low connection strength between E-cells (c_{ee} = 0.001) and high connection strength between I-cells (c_{ii} = 0.200), while keeping connectivity between E-to-I-cells (c_{ei} = 0.050) and I-to-E-cells (c_{ie} = 0.010) at a moderate level. These values were in line with previous studies e.g. [35]. For the connectivity matrix in Fig. 4B and constant input currents (25 pA) to the E-cells and I-cells (Fig. 4C), the model produced oscillatory neuronal activity in the gamma band (Fig. 4D). The membrane potentials of the excitatory neurons were summed to approximate the local field potentials, i.e. the population activity (Fig. 4E). The model generated robust oscillations at 48 Hz as shown in the power spectrum (Fig. 4F).

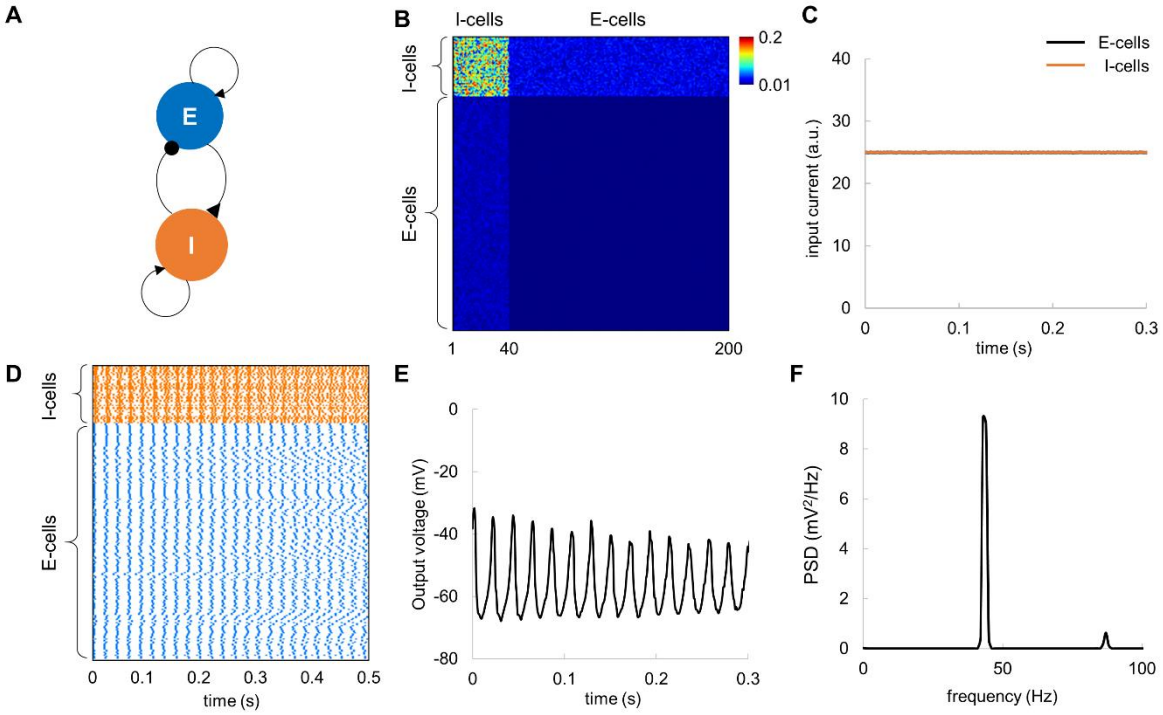

Fig. 4. The PING model with constant input current produces robust neuronal oscillations at around 48 Hz. (A) Neuronal architecture; the simulated network consisted of interconnected E-cells (N=160) and I-cells (N=40). (B) Connectivity matrix between E-cells and I-cells. (C) The inputs current to E-cells (black) and I-cells (orange) were constant. (D) Spike rastergram for E-cells (blue) and I-cells (orange) shows temporal synchronization among the cells. (E) The mean membrane potential of the E-cells exhibited prominent oscillations. (D) Power spectral density of the mean membrane potential for the E-cells shows a clear peak at 48 Hz.

Broadband input to the model produces a gamma echo at the resonance frequency

In order to estimate the TRF of the network dynamics of the model, we applied broadband input current modelled as a sum of constant current of 16 pA and random (uniform) noise with amplitude of 16 pA to the E-cells and a constant current of 25 pA to I-cells (Fig. 5A). This simulates the LGN input to the area V1 in the visual cortex. For the broadband input current, the model produced neuronal activity (Fig. 5A-D) similar to those of the constant input currents (see, Fig. 4). In the presence of broadband input, spiking activity of E-cells remained highly synchronised (Fig. 5B), so that mean membrane potentials showed oscillations that can be readily observed in population response (Fig. 5C) and as well as in the power-spectral density (Fig. 5D). By computing the TRF between the input broadband

current and output voltage, we observed a gamma echo (Fig. 5E) similar to what we observed in the MEG data. Importantly, the frequency of the echo matched the resonance frequency of the model (Fig. 5F).

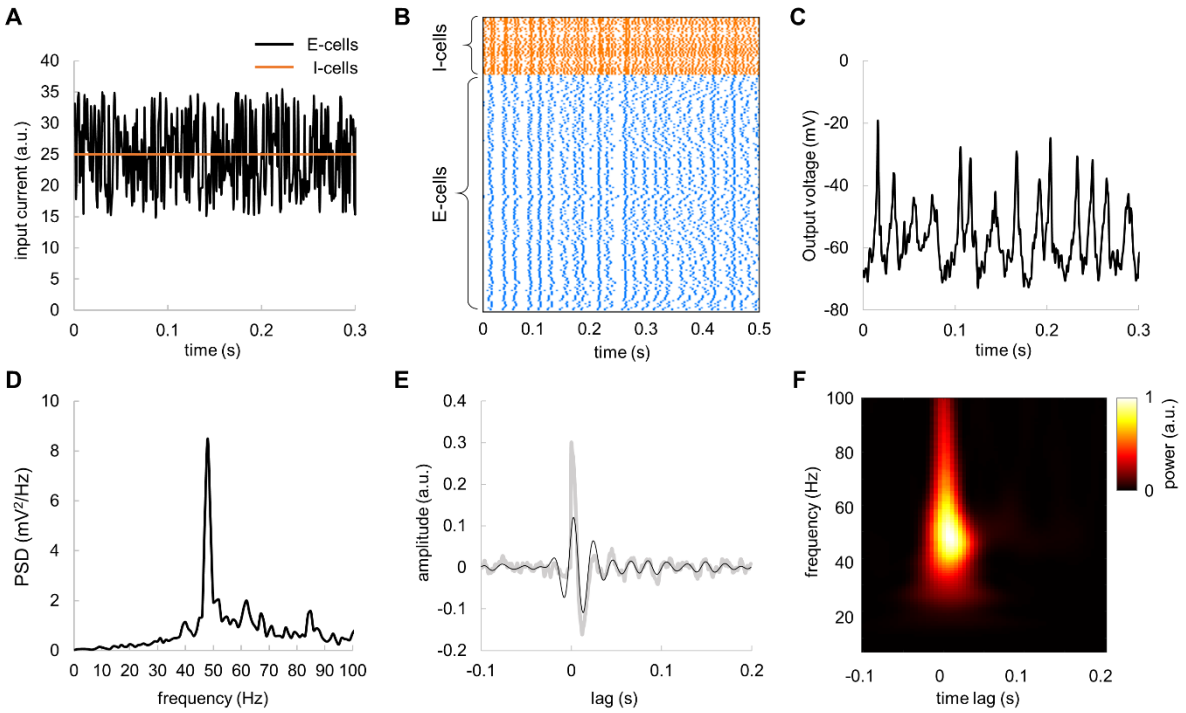

Fig. 5. Broadband input current to E-cells produces damped oscillations in the TRF – the gamma echo. (A) Broadband input current to E-cells (black line) and constant input current to I-cells (orange line). (B) Spike rastergram for E-cells and I-cells for broadband input currrent. (C) The mean membrane potential of the E-cells in response to fluctuating input currents. (D) Power spectral density of mean membrane potentials of the E-cells. (E) TRF with respect to the mean membrane potentials of the E-cells in relation to fluctuating input current. Note the clear “gamma echo”. Gray and black lines depict respectively raw and the filtered TRF (30-60 Hz). (H) Time-frequency representation of power of the TRF.

Oscillatory inputs produce maximum power at the resonance frequency

We further explored the model response by applying an oscillatory input modelled as a sum of constant current of 23 pA and a sinusoidal function with a given frequency (0 – 100 Hz) and an amplitude of 2.5 pA to E-cells while keeping the input current to the I-cells constant at 25 pA (Fig. 6A). The oscillatory input increased synchronization among the E-cells in the gamma band (Fig. 6B) compared to the absence of an oscillatory input (see, Fig. 4D). Figure 6C shows the average membrane potential of the E-cells. The oscillatory input current (mimicking visual stimulation) at the resonance frequency (48 Hz) produced stronger response compared to a response at non-resonance (e.g. 68 Hz) frequency input (Fig. 6D). Interestingly, when driving at non-resonance frequency the model still produced a response at the resonance frequency. To assess the spectral profile of the model in response to different frequencies, we applied a sinusoidal input current ranging from 0 to 100 Hz. The results clearly showed an amplified peak in the power spectral density at the resonance frequency at ~48 Hz (Fig. 6E). It should be noted that the second peak at ~96 Hz was a harmonic of the resonance frequency in the PING model [36].

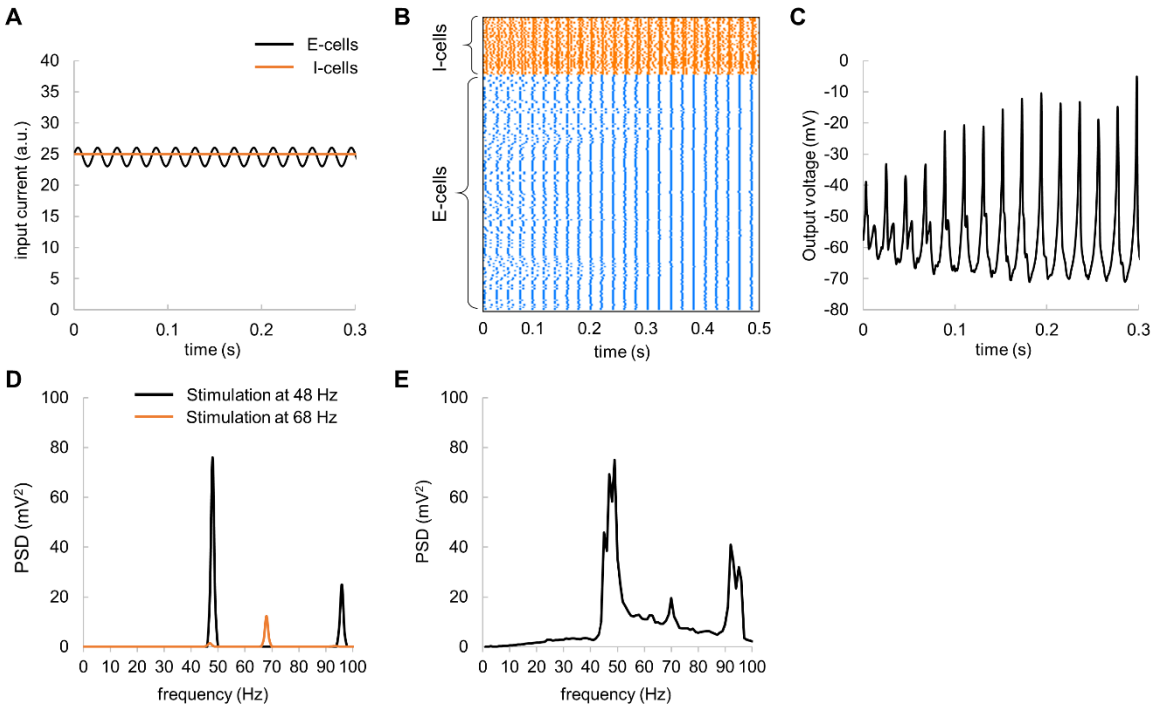

Fig. 6. Oscillatory input current reveals an amplification of oscillatory dynamics at the ~48 Hz resonance frequency. (A) Oscillatory input current to E-cells (black line) and constant current to I-cells (orange line). (B) Spike rastergram for E-cells and I-cells. (C) The mean membrane potential of the E-cells. (D) Example of power spectral density for input current at 48 Hz (resonance frequency, black line) and at 68 Hz (non-resonance, orange line). (E) Power spectral density of mean membrane potential for oscillatory input over multiple frequencies, 0–100 Hz.

Discussion

In this study, we used broadband visual stimulation combined with MEG to assess the dynamical properties of the human visual cortex. We did this by estimating the temporal response function (TRF), i.e. the kernel best explaining the MEG signal from visual cortex when convolved to the broadband visual input. In the TRF we observed an early response limited to the gamma band that we term the *gamma echo*. We also observed the known *perceptual echo* in the alpha band [9]. To explore the neuronal mechanisms producing the gamma echo, we implemented a biophysically plausible pyramidal-interneuron-gamma (PING) model. When driving the model by a broadband input and estimating the respective TRF, we observed a gamma echo similar to the one of the empirical data. Based on these simulations, we suggest that the gamma echo is produced by a network in which the dynamical properties are largely determined by GABAergic interneurons; i.e. a PING-type network adjusted to produce damped oscillations in the gamma band can account for the gamma echo.

Relationship between alpha and gamma echoes

Our findings reveal that both the alpha and gamma echo reflect the intrinsic properties of the visual system but at slightly different times. While the perceptual echo in the alpha band occurs at around 150 ms after stimulus onset, the gamma echo emerges as early as 30 ms and peaks at about 60 ms. Earlier studies have demonstrated that the alpha echo shows

maximum power at the individual alpha frequency [9]. Similarly, we found that the central frequencies of the gamma echo were specific to the participants. Our simulation results showed that the gamma echo of the model was strongly related to the resonance properties of the neuronal network. We suggest that the gamma echo reflects the intrinsic resonance properties of the early visual system.

The gamma echo has not been observed in previous studies applying broadband stimulation (e.g. [9,37] since these studies relied on projectors with a relatively low refresh rate of 100 to 160 Hz. The resulting temporal resolution of 6 – 10 ms corresponds to at least 3 samples for a 48 Hz-cycle, and thus, it does not allow to fully capture gamma-band activity. In this study, we used a projector with a refresh rate of 1440 Hz which allows presenting stimuli with a sub-millisecond temporal resolution allowing for optimally estimating the gamma echo.

A recent study showed that alpha echoes have the characteristics of travelling waves [38]. They further suggest that the spatio-temporal dynamics of the alpha echo is consistent with the timing of the neuronal activity that one might expect for feedforward and feedback communication associated with predictive coding. Indeed, both alpha and gamma oscillations might play a key role in the predictive coding [39,40], and thus, propagation properties associated with the gamma echo may provide crucial insight on the feedforward dynamics associated with predictive coding.

Induced gamma oscillations and gamma echo

Both stationary as we well as contracting visual grating stimuli have been shown to induce robust narrowband endogenous gamma oscillations [41–43]. The characteristics of these oscillations such as amplitude and frequency depend on the parameters of the stimuli (e.g. orientation, spatial frequency, etc.; [42,44,45]). Importantly, human visual gamma oscillations decrease in frequency and increase in power with the application of the GABAergic agonist Lorazepam [20]. This suggests that GABAergic interneurons and thus the classic PING mechanism is responsible for generating the human visual endogenous gamma oscillations.

Recently it was shown that a visual flicker could not entrain endogenous gamma oscillations [46]. This was demonstrated by displaying moving visual gratings superimposed with a constant flicker and flicker frequencies from 50 to 100 Hz were explored. If for instance, the endogenous gamma oscillation frequency for a given participant was 64 Hz, there was no amplification of the gamma oscillations when flickering at that frequency. Rather, the flicker signal and the endogenous gamma oscillations seemed to co-exist. This suggests that different neuronal populations generate respectively the flicker response and the endogenous gamma oscillations. This does however pose an interesting question: what is the relationship between the endogenous gamma oscillations and the gamma echo, given that PING-mechanisms seems to be responsible for both types of dynamics? We propose that the gamma echo is produced by early visual cortex (most likely V1) whereas the endogenous gamma oscillations are produced slightly down-stream (e.g. V2). This scheme is indeed supported by source modelling which localized the generators of the flicker response and the gamma oscillations in neighbouring but different areas [46]. It should also be noted that the frequency of the grating induced endogenous gamma oscillations typically are in the range of 45 to 80 Hz [42,43,46]; and the gamma echo is consistently in the very lower end (~48 Hz) of this range. Interestingly, Gulbinaite and colleagues [47] found a resonance peak at about 48 Hz when driving the visual system exploring 3 to 80 Hz range. In conclusion, we do not believe that the gamma echo we here report is reflecting the dynamics of the endogenous gamma oscillations. While the gamma echo can be explained by the dynamics of the PING model, it seems to reflect the properties of a damped oscillator with resonance properties at ~48 Hz located in early visual cortex. This mechanism coexists

with a network slightly downstream in visual cortex which generates endogenous gamma oscillations in the range of about 45 to 80 Hz.

The gamma echo is not related to 50 Hz line noise.

One might be concerned that the gamma echo is partly a consequence of the 50 Hz line noise given the similar frequencies. However, our analysis on magnetometers (see, Fig. S1) clearly demonstrates that suppression of the 50 Hz line noise does not change the characteristics of the gamma echo in any of the participants. Also note that several other studies report on gamma activity in the vicinity of 50 Hz [42,43,48]. Finally, the gamma echo did vary from 46 to 56 Hz over participants. We conclude that the gamma echo is not biased by the 50 Hz line noise.

Conclusion

Using broadband visual input stimuli were here provide evidence for a band-limited temporal response function in the gamma that we term the gamma echo. A computational model showed that a PING-type of mechanism based on a network producing damped oscillations in the gamma band could account for the gamma echo. Nevertheless, the gamma echo is distinct from the mechanism producing endogenous gamma oscillations. The stage is now set for further investigating how the gamma echo is modulated by tasks such as spatial attention as well as uncovering how the echo might propagate in the visual hierarchy.

References

[1] Shadlen MN, Newsome WT. The variable discharge of cortical neurons: Implications for connectivity, computation, and information coding. Journal of Neuroscience 1998;18:3870–96. https://doi.org/10.1523/jneurosci.18-10-03870.1998.

[2] Stein RB, Gossen ER, Jones KE. Neuronal variability: Noise or part of the signal? Nature Reviews Neuroscience 2005;6:389–97. https://doi.org/10.1038/nrn1668.

[3] Shadlen MN. Rate versus Temporal Coding Models. Encyclopedia of Cognitive Science, Chichester: John Wiley & Sons, Ltd; 2006. https://doi.org/10.1002/0470018860.s00372.

[4] Mangun GR, Hillyard SA, Luck SJ. Electrocortical substrates of visual selective attention. In: Meyer DE, Kornblum S, editors. Attention and performance 14: Synergies in experimental psychology, artificial intelligence, and cognitive neuroscience. 1st ed., The MIT Press; 1993, p. 219–43.

[5] Engel AK, Singer W. Temporal binding and the neural correlates of sensory awareness. Trends in Cognitive Sciences 2001;5:16–25. https://doi.org/10.1016/S1364-6613(00)01568-0.

[6] von der Malsburg C. The what and why of binding: The modeler's perspective. Neuron 1999;24:95–104. https://doi.org/10.1016/S0896-6273(00)80825-9.

[7] Bressler SL. Interareal synchronization in the visual cortex. Behavioural Brain Research 1996;76:37–49. https://doi.org/10.1016/0166-4328(95)00187-5.

[8] Varela F, Lachaux JP, Rodriguez E, Martinerie J. The brainweb: Phase synchronization and large-scale integration. Nature Reviews Neuroscience 2001;2:229–39. https://doi.org/10.1038/35067550.

[9] Vanrullen R, MacDonald JSP. Perceptual echoes at 10 Hz in the human brain. Current Biology 2012;22:995–9. https://doi.org/10.1016/j.cub.2012.03.050.

[10] Tiesinga P, Sejnowski TJ. Cortical Enlightenment: Are Attentional Gamma Oscillations Driven by ING or PING? Neuron 2009;63:727–32. https://doi.org/10.1016/j.neuron.2009.09.009.

[11] Wang XJ, Buzsáki G. Gamma oscillation by synaptic inhibition in a hippocampal interneuronal network model. Journal of Neuroscience 1996;16:6402–13. https://doi.org/10.1523/jneurosci.16-20-06402.1996.

[12] Whittington MA, Traub RD, Kopell N, Ermentrout B, Buhl EH. Inhibition-based rhythms: Experimental and mathematical observations on network dynamics. International Journal of Psychophysiology, vol. 38, Int J Psychophysiol; 2000, p. 315–36. https://doi.org/10.1016/S0167-8760(00)00173-2.

[13] Traub R, Whittington M. Cortical Oscillations in Health and Disease. Oxford University Press; 2010. https://doi.org/10.1093/acprof:oso/9780195342796.001.0001.

[14] van Vreeswijk C, Abbott LF, Bard Ermentrout G. When inhibition not excitation synchronizes neural firing. Journal of Computational Neuroscience 1994;1:313–21. https://doi.org/10.1007/BF00961879.

[15] Gerstner W, van Hemmen JL, Cowan JD. What Matters in Neuronal Locking? Neural Computation 1996;8:1653–76. https://doi.org/10.1162/neco.1996.8.8.1653.

[16] Whittington MA, Traub RD, Jefferys JGR. Synchronized oscillations in interneuron networks driven by metabotropic glutamate receptor activation. Nature 1995;373:612–5. https://doi.org/10.1038/373612a0.

[17] Cardin JA, Carlén M, Meletis K, Knoblich U, Zhang F, Deisseroth K, et al. Driving fast-spiking cells induces gamma rhythm and controls sensory responses. Nature 2009;459:663–7. https://doi.org/10.1038/nature08002.

[18] Tiesinga PHE. Motifs in health and disease: The promise of circuit interrogation by optogenetics. European Journal of Neuroscience 2012;36:2260–72. https://doi.org/10.1111/j.1460-9568.2012.08186.x.

[19] Adesnik H, Scanziani M. Lateral competition for cortical space by layer-specific horizontal circuits. Nature 2010;464:1155–60. https://doi.org/10.1038/nature08935.

[20] Lozano-Soldevilla D, ter Huurne N, Cools R, Jensen O. GABAergic modulation of visual gamma and alpha oscillations and its consequences for working memory performance. Current Biology 2014;24:2878–87. https://doi.org/10.1016/j.cub.2014.10.017.

[21] Muthukumaraswamy SD, Edden RAE, Jones DK, Swettenham JB, Singh KD. Resting GABA concentration predicts peak gamma frequency and fMRI amplitude in response to visual stimulation in humans. Proceedings of the National Academy of Sciences of the United States of America 2009;106:8356–61. https://doi.org/10.1073/pnas.0900728106.

[22] Gaetz W, Edgar JC, Wang DJ, Roberts TPL. Relating MEG measured motor cortical oscillations to resting γ-Aminobutyric acid (GABA) concentration. NeuroImage 2011;55:616–21. https://doi.org/10.1016/j.neuroimage.2010.12.077.

[23] Edden RAE, Muthukumaraswamy SD, Freeman TCA, Singh KD. Orientation discrimination performance is predicted by GABA concentration and gamma oscillation frequency in human primary visual cortex. Journal of Neuroscience 2009;29:15721–6. https://doi.org/10.1523/JNEUROSCI.4426-09.2009.

[24] Cousijn H, Haegens S, Wallis G, Near J, Stokes MG, Harrison PJ, et al. Resting GABA and glutamate concentrations do not predict visual gamma frequency or amplitude. Proceedings of the National Academy of Sciences of the United States of America 2014;111:9301–6. https://doi.org/10.1073/pnas.1321072111.

[25] Kujala J, Jung J, Bouvard S, Lecaignard F, Lothe A, Bouet R, et al. Gamma oscillations in V1 are correlated with GABAA receptor density: A multi-modal MEG and Flumazenil-PET study. Scientific Reports 2015;5:16347. https://doi.org/10.1038/srep16347.

[26] Zhigalov A, Jensen O. Alpha oscillations do not implement gain control in early visual cortex but rather gating in parieto-occipital regions. Human Brain Mapping 2020;41:5176–86. https://doi.org/10.1002/hbm.25183.

[27] Kleiner M, Brainard D, Pelli D, Ingling A, Murray R, Broussard C. What's new in psychtoolbox-3. vol. 36. [Pion Ltd.]; 2007.

[28] Virtanen P, Gommers R, Oliphant TE, Haberland M, Reddy T, Cournapeau D, et al. SciPy 1.0: fundamental algorithms for scientific computing in Python. Nature Methods 2020;17:261–72. https://doi.org/10.1038/s41592-019-0686-2.

[29] Crosse MJ, di Liberto GM, Bednar A, Lalor EC. The multivariate temporal response function (mTRF) toolbox: A MATLAB toolbox for relating neural signals to continuous stimuli. Frontiers in Human Neuroscience 2016;10:604. https://doi.org/10.3389/fnhum.2016.00604.

[30] Taulu S, Simola J. Spatiotemporal signal space separation method for rejecting nearby interference in MEG measurements. Physics in Medicine and Biology 2006;51:1759–68. https://doi.org/10.1088/0031-9155/51/7/008.

[31] Oostenveld R, Fries P, Maris E, Schoffelen J-M. FieldTrip: Open source software for advanced analysis of MEG, EEG, and invasive electrophysiological data. Computational Intelligence and Neuroscience 2011;2011:156869. https://doi.org/10.1155/2011/156869.

[32] Izhikevich EM. Simple model of spiking neurons. IEEE Transactions on Neural Networks 2003;14:1569–72. https://doi.org/10.1109/TNN.2003.820440.

[33] Hämäläinen M, Hari R, Ilmoniemi RJ, Knuutila J, Lounasmaa O v. Magnetoencephalography theory, instrumentation, and applications to noninvasive studies of the working human brain. Reviews of Modern Physics 1993;65:413–97. https://doi.org/10.1103/RevModPhys.65.413.

[34] Gramfort A, Luessi M, Larson E, Engemann DA, Strohmeier D, Brodbeck C, et al. MEG and EEG data analysis with MNE-Python. Frontiers in Neuroscience 2013;7. https://doi.org/10.3389/fnins.2013.00267.

[35] Quax S, Jensen O, Tiesinga P. Top-down control of cortical gamma-band communication via pulvinar induced phase shifts in the alpha rhythm. PLoS Computational Biology 2017;13. https://doi.org/10.1371/journal.pcbi.1005519.

[36] Lee S, Jones SR. Distinguishing mechanisms of gamma frequency oscillations in human current source signals using a computational model of a laminar neocortical network. Frontiers in Human Neuroscience 2013;7. https://doi.org/10.3389/fnhum.2013.00869.

[37] Jia J, Liu L, Fang F, Luo H. Sequential sampling of visual objects during sustained attention. PLoS Biology 2017;15. https://doi.org/10.1371/journal.pbio.2001903.

[38] Alamia A, VanRullen R. Alpha oscillations and traveling waves: Signatures of predictive coding? PLoS Biology 2019;17. https://doi.org/10.1371/journal.pbio.3000487.

[39] Bastos AM, Lundqvist M, Waite AS, Kopell N, Miller EK. Layer and rhythm specificity for predictive routing. Proceedings of the National Academy of Sciences 2020;117:202014868. https://doi.org/10.1073/pnas.2014868117.

[40] Bastos AM, Usrey WM, Adams RA, Mangun GR, Fries P, Friston KJ. Canonical Microcircuits for Predictive Coding. Neuron 2012;76:695–711. https://doi.org/10.1016/j.neuron.2012.10.038.

[41] Muthukumaraswamy SD, Singh KD, Swettenham JB, Jones DK. Visual gamma oscillations and evoked responses: Variability, repeatability and structural MRI correlates. NeuroImage 2010;49:3349–57. https://doi.org/10.1016/j.neuroimage.2009.11.045.

[42] van Pelt S, Fries P. Visual stimulus eccentricity affects human gamma peak frequency. NeuroImage 2013;78:439–47. https://doi.org/10.1016/j.neuroimage.2013.04.040.

[43] Hoogenboom N, Schoffelen JM, Oostenveld R, Parkes LM, Fries P. Localizing human visual gamma-band activity in frequency, time and space. NeuroImage 2006;29:764–73. https://doi.org/10.1016/j.neuroimage.2005.08.043.

[44] Hermes D, Miller KJ, Wandell BA, Winawer J. Stimulus dependence of gamma oscillations in human visual cortex. Cerebral Cortex 2015;25:2951–9. https://doi.org/10.1093/cercor/bhu091.

[45] Muthukumaraswamy SD, Singh KD. Visual gamma oscillations: The effects of stimulus type, visual field coverage and stimulus motion on MEG and EEG recordings. NeuroImage 2013;69:223–30. https://doi.org/10.1016/j.neuroimage.2012.12.038.

[46] Duecker K, Gutteling TP, Herrmann CS, Jensen O. No evidence for entrainment: endogenous gamma oscillations and 1 rhythmic flicker responses coexist in visual cortex. BioRxiv 2020:2020.09.02.279497. https://doi.org/10.1101/2020.09.02.279497.

[47] Gulbinaite R, Roozendaal DHM, VanRullen R. Attention differentially modulates the amplitude of resonance frequencies in the visual cortex. NeuroImage 2019;203:116146. https://doi.org/10.1016/j.neuroimage.2019.116146.

[48] Swettenham JB, Muthukumaraswamy SD, Singh KD. Spectral properties of induced and evoked gamma oscillations in human early visual cortex to moving and stationary

stimuli. Journal of Neurophysiology 2009;102:1241–53. https://doi.org/10.1152/jn.91044.2008.

Supporting information

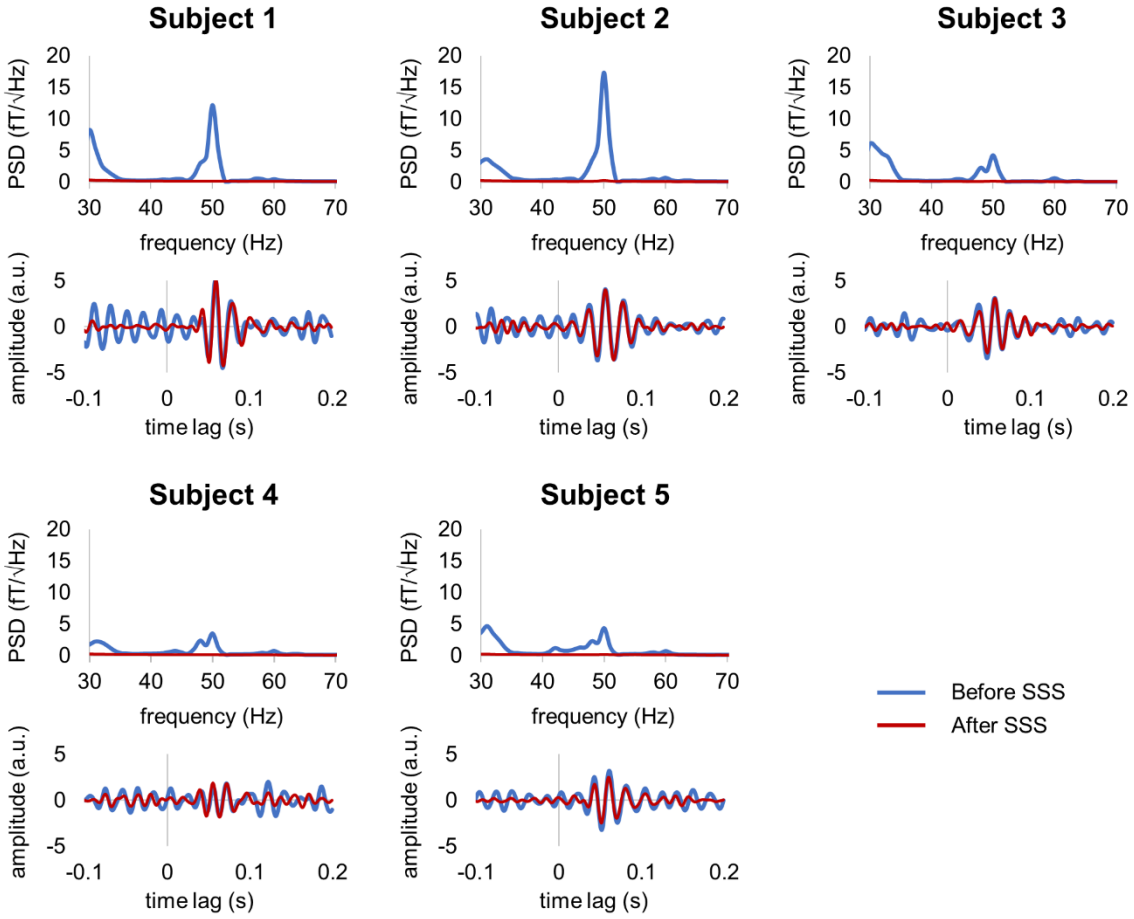

Fig. S1. Suppression of line noise in data does not change the characteristics of the gamma echo in representative magnetometers. Each panel shows the power spectral density (PSD) and TRF for individual participants before (blue line) and after (orange line) applying the SSS method to suppress 50 Hz line noise. The echos remain strong after the 50 Hz line noise is suppressed.